
Supporting Information

Engineering Mn Atomic Sites in Multi-Dimensional Nitrogen-Doped Carbon for Highly Efficient Oxygen Reduction Reaction

Huixin Ma[a,‡], Daijie Deng[a,‡], Honghui Zhang[a], Feng Chen[b,*], Junchao Qian[b], Henan Li[a], Li Xu[a,*]

[a]*Institute for Energy Research, School of Chemistry and Chemical Engineering, School of Materials Science and Engineering, Key Laboratory of Zhenjiang, Jiangsu University, Zhenjiang 212013, P. R. China.*

[b.] *Jiangsu Key Laboratory for Environment Functional Materials, Suzhou University of Science and Technology, Suzhou 215009, P. R. China.*

‡These authors contributed equally.

Email: chenfeng@mail.usts.edu.cn (F. Chen); xulichem@ujs.edu.cn (L. Xu)

Experimental materials

Urea (AR), manganese(II) chloride tetrahydrate ($MnCl_2·4H_2O$, AR), potassium hydroxide (KOH, AR), potassium thiocyanate (KSCN, AR), absolute ethyl alcohol (C_2H_5OH) and hydrochloric acid (HCl, 36%~38%) were produced from Sin pharm Chemical Reagent Co., Ltd (Shanghai, China). Bacterial fiber gel (dispersions, 0.65 wt%, 1% NaOH pretreatment) was purchased from Qihong Technology Co., Ltd. (Guilin, China). Commercial 20 wt% Pt/C was produced from Alfa Aesar (China) Chemicals Co. Ltd (Shanghai). Nafion solution (10 wt%) was purchased from Aladdin Industrial Corporation (Shanghai, China). All chemicals can be used directly without further purification.

Synthesis of Mn-NC

Typically, urea (2 g) was placed in a tubular furnace, heated to 600 ºC with a heating rate of 2 °C min^{-1} in nitrogen atmosphere, and kept for 2 h to obtain pale yellow carbon nitride. The bacterial fiber gel dispersions (10 g, 0.65 wt%) was diluted into 10 mL deionized water. g-C_3N_4 (0.2 g) was dispersed into 10 mL deionized water. Then, the uniformly dispersed g-C_3N_4 dispersion was added into the diluted bacterial fiber gel dispersion under magnetic agitation. After being continuously stirred for 3 h, the mixed dispersion was labeled as the dispersion A. Next, $MnCl_2·4H_2O$ (0.2 mmol) was dissolved into 8 mL deionized water, and then added drop by drop to the dispersion A. After being stirred for 6 h, the Mn^{2+}/g-C_3N_4/gel mixture was dried with vacuum freezing drying technology at –80 °C and then turned into the Mn^{2+}/g-C_3N_4/aerogel. The porcelain crucible containing Mn^{2+}/g-C_3N_4/aerogel was placed into the sealed quartz tube with a vacuum of –0.1 M Pa at 900 °C. After being held for 10 min, the sealed quartz tube was quickly taken out from the muffle furnace and naturally cooled at room temperature. Then, the sample in sealed quartz tube was dispersed into 0.5 M HCl and stirred for 6 h. The powder sample treated with HCl was collected by filtrated and washed to pH≈7 with deionized water. Finally, Mn-NC was obtained after being calcined the powder sample with the same calcination method as above.

The NC catalyst was also prepared with the same process without $MnCl_2·4H_2O$.

Characterization

The phases of samples were characterized by X-ray powder diffraction (XRD-6100) in 2θ range of 10° to 80° with scanning rate of 3° min^{-1} with Cu 145 Kα radiation (λ=0.1541 nm). The surface area was determined with the Brunauer-Emmett-Teller (BET, Micromerit-ics Instrument Corporation, USA). Raman spectroscopy was conducted and recorded using the confocal Raman system (RTS2, Zolix) with a 532 nm excitation source. Field-emission scanning electron microscopy (FE-SEM) and transmission electron microscopy (TEM) images were obtained on the JEOL JSM-7800F FE-SEM and JEOL JEM-2010 TEM. High-angle annular dark-field scanning transmission electron microscopy (HAADF-STEM) images were recorded on JEOL JEM-ARM200F NEOARM atomic resolution analytical electron microscope at 200 kV. X-ray photoelectron spectra (XPS) were obtained with CAE scanning mode (Nexsa, Thermo Fisher) by

using mono Alka (energy:1486.6 eV) X-ray source. Inductively coupled plasma optical emission spectrometry (ICP, PE Avio 200) was used to determine the content of Mn within Mn-NC.

Preparation of working electrodes

Deionized water, C_2H_5OH and 10 wt % Nafion were mixed with a volume ratio of 5:5:0.2 to disperse the prepared catalyst by ultrasound and then obtain the catalyst ink. The working electrodes were prepared by dropping the catalyst ink on the surface of rotating disk electrode (RDE, diameter: 3 mm) or rotating ring disk electrode (RRDE, diameter: 4 mm with a Pt ring). Then, RDE or RRDE electrodes were dried naturally in the air at room temperature. Finally, the catalyst loading on the RDE and RRDE electrode surfaces was determined to be 0.35 mg cm^{-1} and 0.2 mg cm^{-1}, respectively.

Electrochemical measurements

The electrochemical measurements were carried out on the CHI 760E electrochemical workstation (CHI Shanghai, Inc.) with standard three-electrode system. In the three-electrode system, the glassy carbon electrode and Ag/AgCl electrode (in 3 M KCl aqueous) were used as the counter electrode and the reference electrode, respectively.

Cyclic voltammetry (CV) curves were recorded in O_2-saturated KOH (0.1 M) solution with the scan rate of 100 mV s^{-1}. The linear sweep volt-ampere (LSV) curves were measured with the rotation speed of 1600 rpm and the scan rate of 10 mV s^{-1}.

All potentials were converted to reversible hydrogen electrode (RHE) potentials according to the Nernst equation ($E_{RHE} = E_{Ag/AgCl} + 0.210\ V + 0.059 \times pH$).

The K–L plot was calculated based on the Koutecky–Levich equation:

$$\frac{1}{J}=\frac{1}{J_L}+\frac{1}{J_K}=\frac{1}{B\omega^{1/2}}+\frac{1}{J_K} \tag{2}$$

$$B = 0.62nFC_0(D_0)^{2/3}\upsilon^{-1/6} \tag{3}$$

$$j_k = nFkC_0 \tag{4}$$

The symbols are notated in the equation as follows:

J is the measured current density. J_K and J_L are the kinetic and limiting current densities, respectively. ω is the rotation speed of electrode (rpm) of RDE or RRDE. n is the electron transfer number for ORR. F is Faraday constant (96485 C mol^{-1}). $D_{(O_2)}$ is the diffusion coefficient of O_2 in 0.1 M KOH (1.9×10^{-5} cm^2 s^{-1}). ν is the kinematic viscosity (0.01 cm^2 s^{-1}). $C_{(O_2)}$ is the bulk concentration of O_2 in the aqueous solution (1.2×10^{-6} mol cm^{-3}).

Tafel slope were calculated according to the formula ($\eta = b \log(j/j_0)$) based on LSV curves. The η is the overpotential. The j is the current density. The j_0 is the exchange current density.

RRDE tests were measured with the rotation speed of 1600 rpm (scan rate: 10 mV s^{-1}). The ring electrode potential was set to 1.25 V (vs. RHE) to oxidize H_2O_2 from the disk electrode.

Hydrogen peroxide yields (H_2O_2 %) and electron transfer numbers (n) were determined by the following equations:

$$n = 4 \times \frac{I_d}{I_d + I_r / N} \tag{5}$$

$$HO_2^-(\%) = 200 \times \frac{I_r / N}{I_d + I_r / N} \tag{6}$$

where I_r and I_d are respectively ring and disk currents. N is collection efficiency of the Pt ring (0.37).

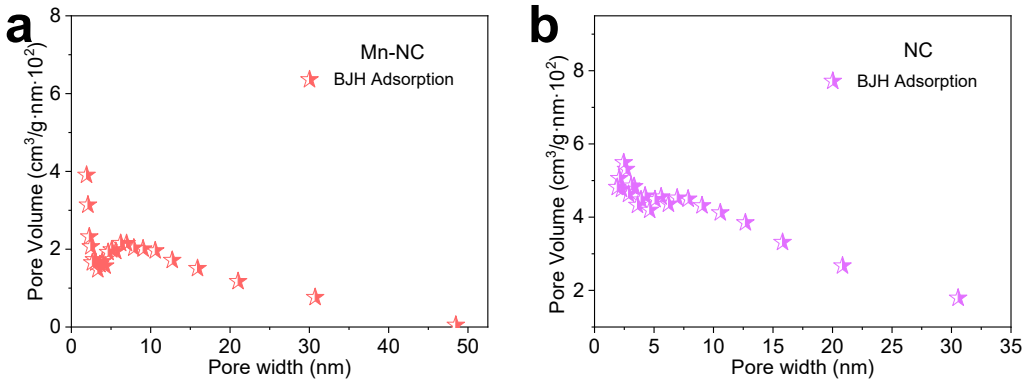

Figure S1. The pore size distributions of Mn-NC (a) and NC (b).

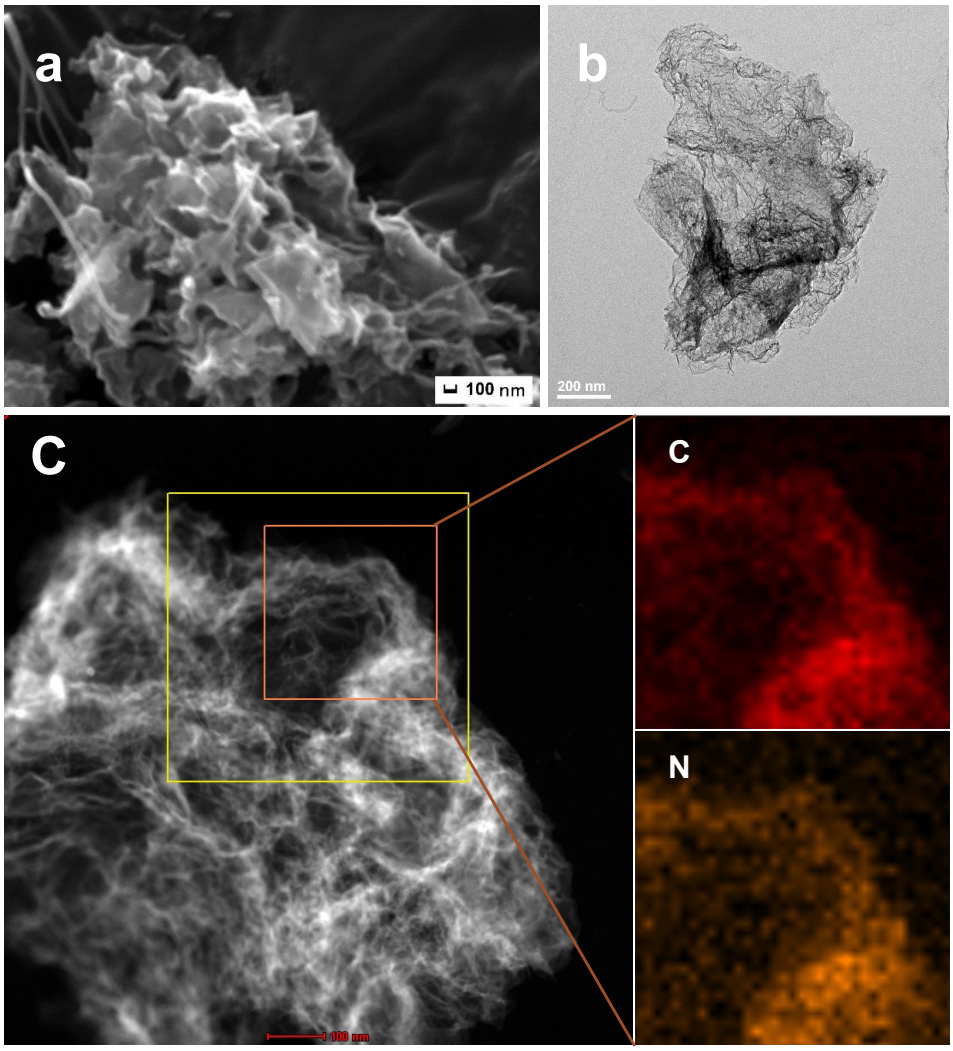

Figure S2. (a) SEM and (b) TEM images of NC; (c) EDX mapping images of NC for C and N.

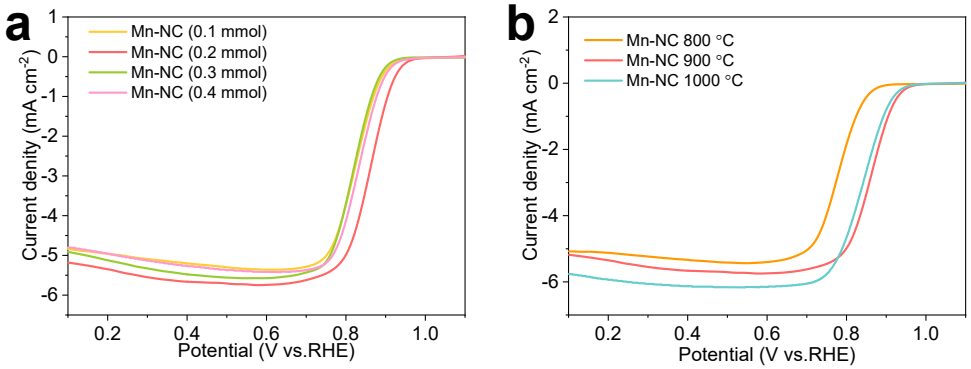

Figure S3. ORR activity of Mn-NC catalysts with different (a) Mn contents and (b) pyrolysis temperatures in O_2-saturated 0.1 M KOH at a rotation rate of 1600 rpm.

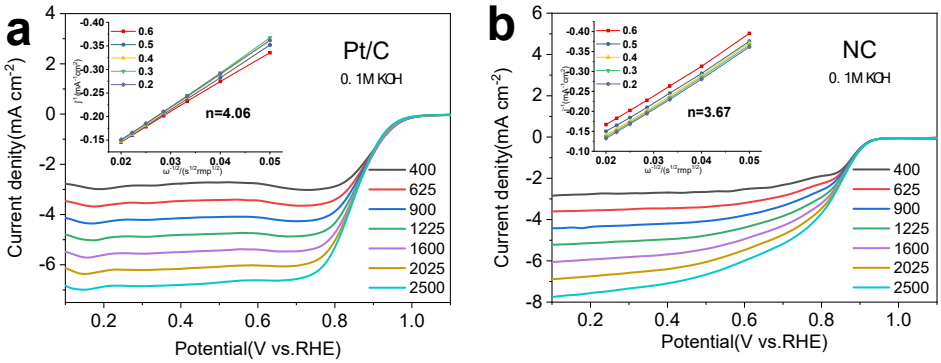

Figure S4. LSV curves of (a) Pt/C and (b) NC at different rotation speeds range (400−2500 rpm, inset shows the corresponding K-L plots).

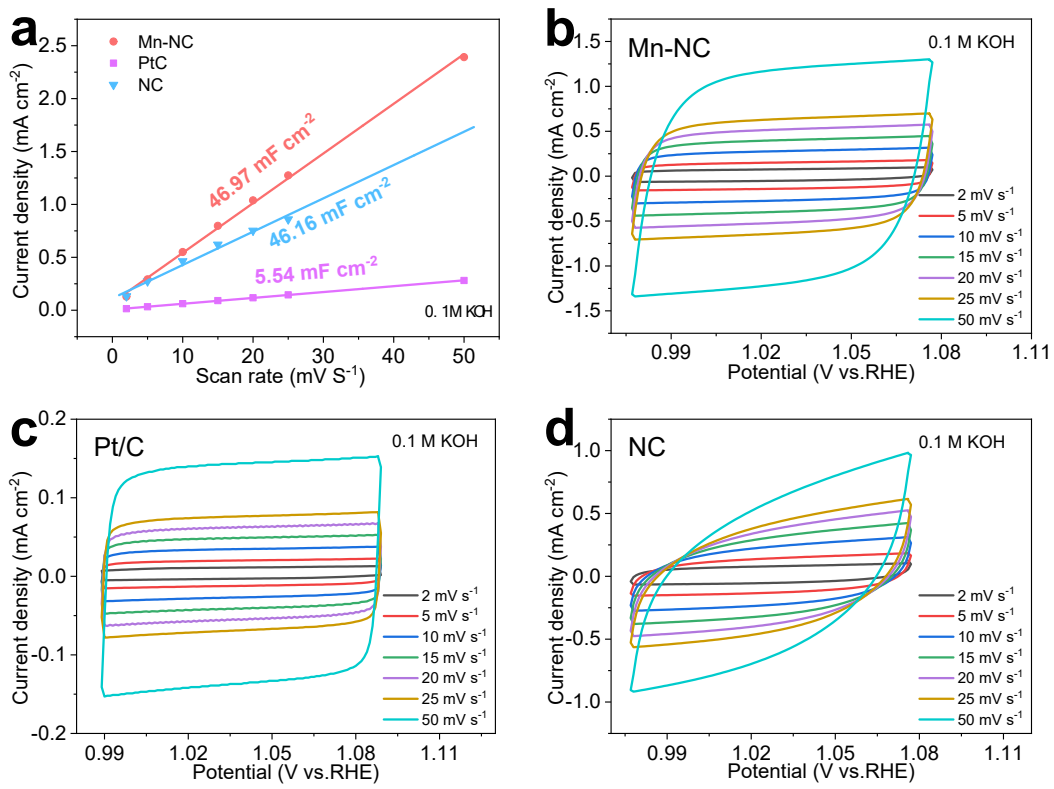

Figure S5. (a) The measured capacitive currents plotted as a function of scan rate of Mn-NC, Pt/C, and NC in 0.1 M KOH. CV curves of (b) Mn-NC, (c) Pt/C, and (d) NC in 0.1 M KOH with different scan rate of 2, 5, 10, 15, 20, 25 and 50 mV s^{-1}.

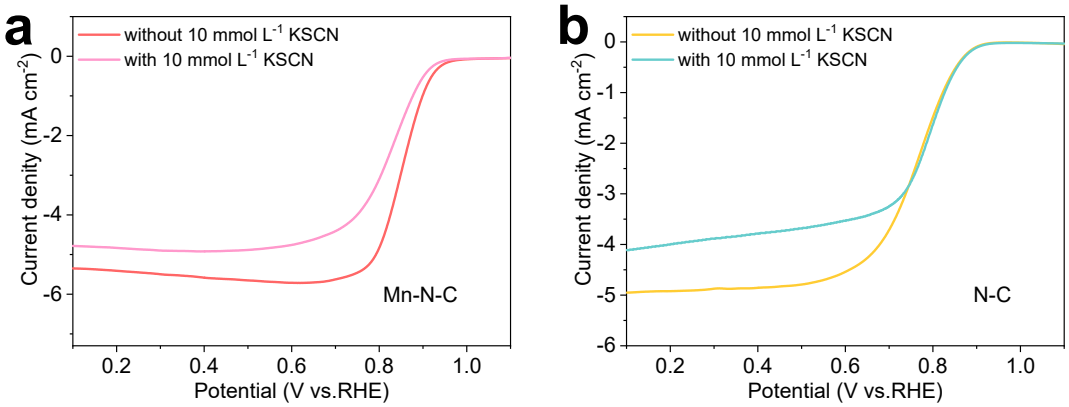

Figure S6. LSV curves of ORR on toxicity tests of SCN^- for (a) Mn-NC and (b) NC.

Table S1. The Mn content of Mn-NC catalyst tested by ICP and XPS methods in this work, and comparison of major metal contents with monodispersed transition metal-N-C catalysts in reported literatures.

Catalyst	Main element	XPS results (at.%)	ICP results (wt.%)	Ref.
Mn-NC	Mn	1.16	1.10	This work
Cu/Zn-NC	Cu	/	0.34	1
	Zn	/	0.38	
Ni/Cu−N−C	Ni	/	0.27	2
	Cu	/	0.31	
Fe-Z_8NC&NaCl	Fe	/	0.42	3
CoSA/N,S-HCS	Co	/	0.82	4
S-Cu-ISA/SNC	Cu	/	0.73	5
Fe/OES	Fe	/	0.11	6
Fe/BCS	Fe	/	0.09	
MF-Fe-800	Fe	/	1.01	7
Fe-N-C	Fe	/	0.2	8
Fe-N-C-950	Fe	/	0.32	9
FeCo-NGS	Fe	/	0.62	10
FeCo-NGS	Co	/	0.25	

Table S2. The comparation of ORR half-wave potential for the Mn-NC catalyst in this work with those of Mn based catalysts in reported literatures.

Catalysts	Half-wave potential (V vs. RHE)	Ref.
Mn-NC	0.88	This work
Mn-SA	0.87	11
Mn-N-C900	0.88	12
Mn/C–NO	0.86	13
MnNC-PDA-700	0.87	14
MnVOx@N-Rgo	0.80	15
$Mn_7C_3/V_8C_7/MnO$	0.82	16
D-AC@2Mn-4Co	0.80	17
PT-MnN_4	0.88	18

References

1. M.M. Tong, F.F. Sun, Y. Xie, Y. Wang, Y.Q. Yang, C.G. Tian, L. Wang and H.G. Fu, *Angew. Chem. Int. Ed.*, 2021, **60**, 14005.

2. H.Y. Cheng, X.M. Wu, M.M. Feng, X.C. Li, G.P. Lei, Z.H. Fan, D.W. Pan, F.J. Cui and G.H. He, *ACS Catal.*, 2021, **11**, 12673–12681.

3. Y.J. Cao, H.Y. Peng, S.Q. Chu, Y.T. Tang, C.J. Huang, Z.L. Wang, F. Liu, J.S. Wu, B. Shan and R. Chen, *Chem. Eng. J.*, 2021, **420**, 129713.

4. Z.Y. Zhang, X.X. Zhao, S.B. Xi, L.L. Zhang, Z.X. Chen, Z.P. Zeng, M. Huang, H.B. Yang, B. Liu, S.J. Pennycook and P. Chen, *Adv. Energy Mater.*, 2020, **10**, 2002896.

5. H.S. Shang, X.Y. Zhou, J.C. Dong, A. Li, X. Zhao, Q.H. Liu, Y. Lin, J.J. Pei, Z. Li, Z.L. Jiang, D.N. Zhou, L.R. Zheng, Y. Wang, J. Zhou, Z.K. Yang, R. Cao, R. Sarangi, T.T. Sun, X. Yang, X.S. Zheng, W.S. Yan, Z.B. Zhuang, J. Li, W.X. Chen, D.S. Wang, J.T. Zhang and Y.D. Li, *Nat. Commun.*, 2020, **11**, 3049.

6. C.C. Hou, L.l. Zou, L.M. Sun, K.X. Zhang, Z. Liu, Y.W. Li, C.X. Li, R.Q. Zou, J.H. Yu and Q. Xu, *Angew. Chem. Int. Ed.*, 2020, **59**, 7384–7389.

7. H.T. Chung, D.A. Cullen, D. Higgins, B.T. Sneed, E.F. Holby, K.L. More and P. Zelenay, *Science*, 2017, **357**, 479–484.

8. B. Lu, T.J. Smart, D. Qin, J.E. Lu, N. Wang, L. Chen, Y. Peng, Y. Ping and S. Chen, *Chem. Mater.*, 2017, **29**, 5617–5628.

9. M. Xiao, J. Zhu, L. Ma, Z. Jin, J. Ge, X. Deng, Y. Hou, Q. He, J. Li, Q. Jia, S. Mukerjee, R. Yang, Z. Jiang, D. Su, C. Liu and W. Xing, *ACS Catal.*, 2018, **8**, 2824–2832.

10. C. Chen, Y.F. Li, D. Cheng, H. He and K. Zhou, *ACS Appl. Mater. Interfaces*, 2020, **12**, 40415–40425.

11. Z. Lin, H. Huang, L. Cheng, Y. Yang, R. Zhang and Q. Chen, *ACS Sustain. Chem. Eng.*, 2019, **8**, 427–434.

12. Y. Wang, X. Zhang, S. Xi, X. Xiang, Y. Du, P. Chen, D. Lyu, S. Wang, Z. Q. Tian and P. K. Shen, *ACS Sustain. Chem. Eng.*, 2020, **8**, 9367–9376.

13. Y. Yang, K. Mao, S. Gao, H. Huang, G. Xia, Z. Lin, P. Jiang, C. Wang, H. Wang and Q. Chen, *Adv. Mater.*, 2018, **30**, 1801732.

14. H. Tian, X. Cui, H. Dong, G. Meng, F. Kong, Y. Chen, L. Peng, C. Chen, Z. Chang and J. Shi, *Energy Storage Mater.*, 2021, **37**, 274–282.

15. X. Xing, R. Liu, K. Cao, U. Kaiser, G. Zhang and C. Streb, *ACS Appl. Mater. Interfaces*, 2018, **10**, 44511–44517.

16. X. Xing, R. Liu, K. Cao, U. Kaiser and C. Streb, *Chem. Eur. J.*, 2019, **25**, 11098–11104.

17. H. Tian, L. Zeng, Y. Huang, Z. Ma, G. Meng, L. Peng, C. Chen, X. Cui and J. Shi, *Nano-Micro Lett.*, 2020, **12**, 161.

18. L. Yan, L. Xie, X. Wu, M. Qian, J. Chen, Y. Zhong and Y. Hu, *Carbon Energy*, 2021, 1–10.